Supporting Information

Stable Thiophosphate-based All-Solid-State Lithium Batteries through Conformally Interfacial Nano Coating

Daxian Cao,[†,#] Yubin Zhang,[‡,#] Adelaide M. Nolan,[§] Xiao Sun,[†] Chao Liu,[†] Jinzhi Sheng,[†] Yifei Mo,[§,*] Yan Wang,[‡,*] Hongli Zhu[†,*]

[†]Department of Mechanical and Industrial Engineering, Northeastern University, Boston, Massachusetts 02115, United States

[‡]Department of Mechanical Engineering, Worcester Polytechnic Institute, Worcester, Massachusetts 01609, United States

[§]Department of Materials Science and Engineering, University of Maryland, College Park, MD 20742, United States

[#]These authors contributed equally

*: Correspondence: h.zhu@neu.edu (H.Z.); yanwang@wpi.edu (Y.W.); yfmo@umd.edu (Y.M.)

1. Ionic conductivity of LLSTO

Ionic conductivity was assessed using electrochemical impedance spectroscopy. **Figure S1** showed representative Nyquist plots of complex impedance for the amorphous LLSTO thin films measured in an Ar atmosphere at 30 ºC. The spectra consist of only one semicircle or a part of one semicircle, which was asymmetric in the low frequency range. This asymmetry may be attributed to electrode contribution. In addition, the low-frequency arcs for LLSTO thin films are incomplete because of high interfacial resistance between electrode and thin film. In order to avoid any structure change to these thin films, no extra heat treatment was used to improve the adhesion between the sputtered gold electrodes and the thin films. As discussed in our previous works, the arc in the low-frequency side is associated with the electrode-film interfacial properties, while the arc in the high frequency region is attributed to the lithium ionic conduction in the thin film.

In order to determine the dc conductivities of the amorphous LLSTO thin films, the impedance response was modeled with a fitting equivalent circuit. The thin film response (the high frequency semicircle) was modeled by using a resistor (R) in parallel with a constant phase element (CPE). A Warburg element was used to describe the electrode related contributions for the impedance spectra. The thin film resistance was determined from the complex spectra by fitting experimental data to the equivalent circuit. The dc ionic conductivities were calculated from this effective dc resistance. The ionic conductivities of the amorphous LLTO thin film were obtained by the classical equation:

$$\sigma = \frac{1}{R} \times \frac{L}{S} \quad (1)$$

where R is the thin film resistance (Ω), L is the film thickness (cm) and S is the cross-sectional area that the electric field was applied across. The conductivity at 30 ºC is 8.38×10^{-5} S/cm for amorphous LLSTO thin films. The amorphous LLSTO exhibits a significantly higher conductivity than the un-doped amorphous LLTO.

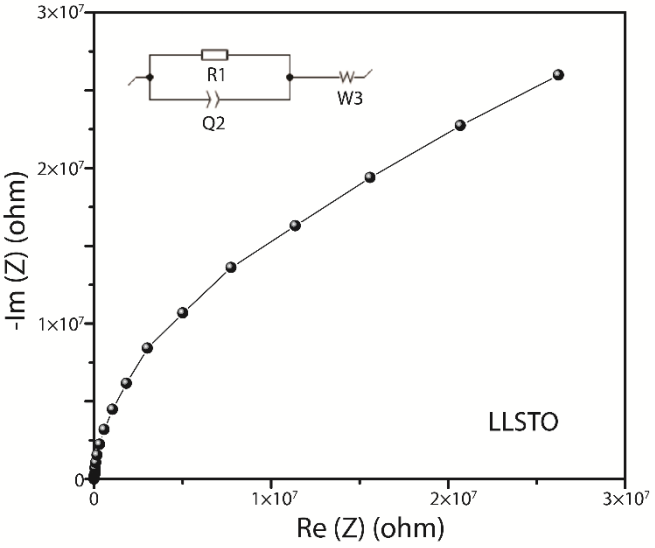

Figure S1. Nyquist plot of LLSTO. Inset shows the equivalent circuit.

2. XRD patterns of Li_6PS_5Cl and Ionic conductivity

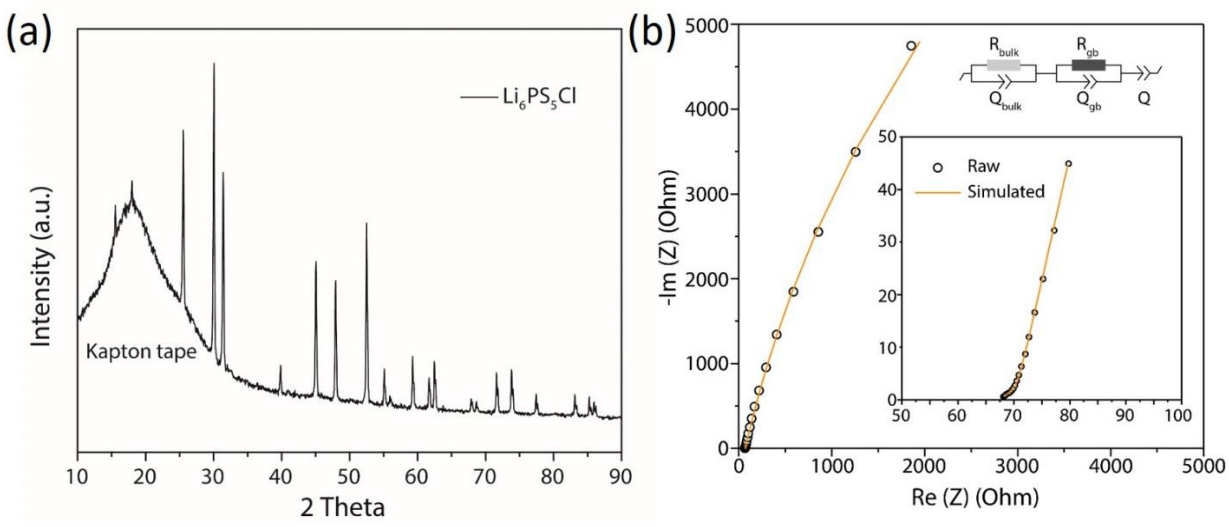

Figure S2. (a) XRD patterns of Li_6PS_5Cl. The bumped peak was derived from the Kapton tape for sample protection. (b) Nyquist plots and fit result of Li_6PS_5Cl. Inset shows the zooming in image at high frequency and equivalent circuit.

3. Diffusion calculation.

The calculation of diffusion is based on the modified Fick's law in previous publication.[1] Because the current rate (C/20) is fairly low for GITT, the well-known Fick's law through Equation (2) can be simplified as Equation (3). The τ is the duration time for each discharge step, and the values of ΔV_s and ΔV_t are extracted from Figure S3, respectively. The R_s is the average radius of each NMC particles, which is around 4.1 μm.

$$D_s = \frac{4}{\pi}\left(\frac{IV_m}{z_A FS}\right)^2\left[\frac{(dE/d\delta)}{(dE/d\sqrt{t})}\right]^2 \quad \left(t \ll \frac{L^2}{D_s}\right) \tag{2}$$

$$D_s = \frac{4}{\pi}\left(\frac{R_s}{3}\right)^2\left[\frac{\Delta V_s}{\Delta V_t}\right]^2 \quad \left(\tau \ll \frac{{R_s}^2}{D_s}\right) \tag{3}$$

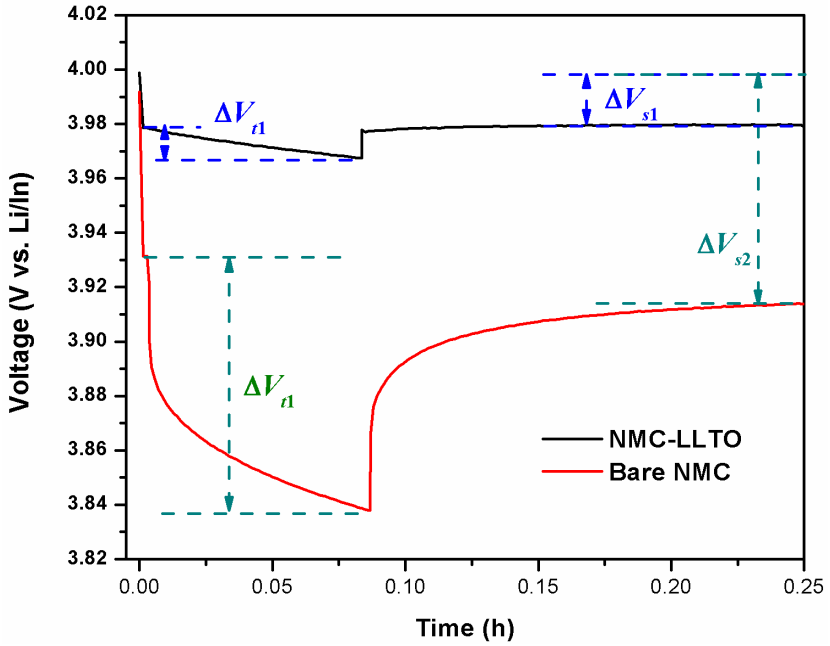

Figure S3. The transient voltage profiles in one discharge pulse. The black line and red line show the voltage response of NMC-LLSTO and Bare NMC, respectively.

4. Optimization of coating conditions

In order to generate uniform LLSTO coating on NMC, the formation of gel is of vital. As shown in **Figure S4a**, without the gel-forming process, the coating layer only partially covered the NMC particles, which was due to the insufficient attraction between NMC particles and LLSTO sol. Therefore, the suspension of NMC in LLSTO sol was placed in ambient air for X hs to form the gel. As a result, a conformal coating on the NMC was achieved due to the intimate attraction (**Figure S4b**). The thickness of the coating layer can be well adjusted by control the ratio of NMC and LLSTO.

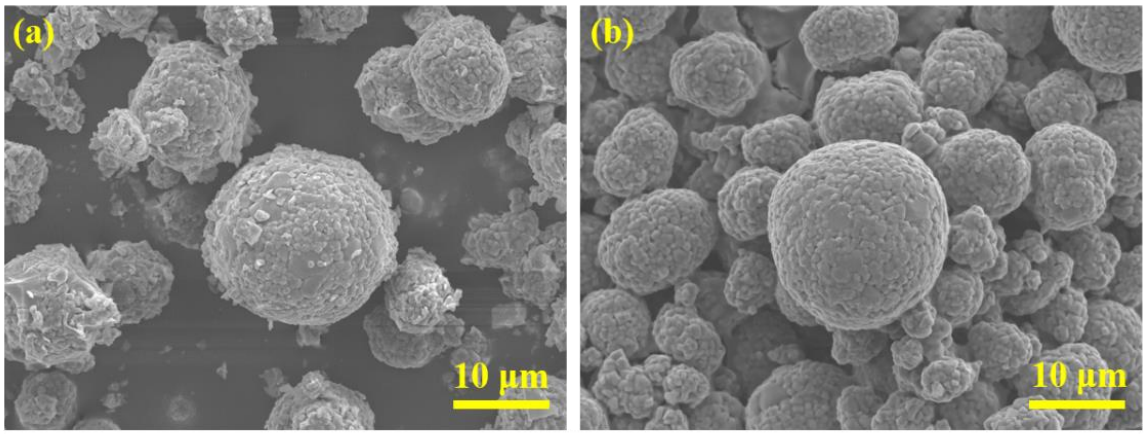

Figure S4. The morphology of NMC-LLSTO: (a) without;(b) with gel-forming process.

5. Morphology of NMC with different coating thickness

Table S1. The ratio of NMC to the LLSTO in coating preparation.

Sample #	NMC (g)	LLSTO (mmol)	NMC:LLSTO (wt%)
1	2	0.25	2.91:1
2	2	0.33	3.87:1
3	2	0.50	5.81:1
4	2	1.00	11.62:1

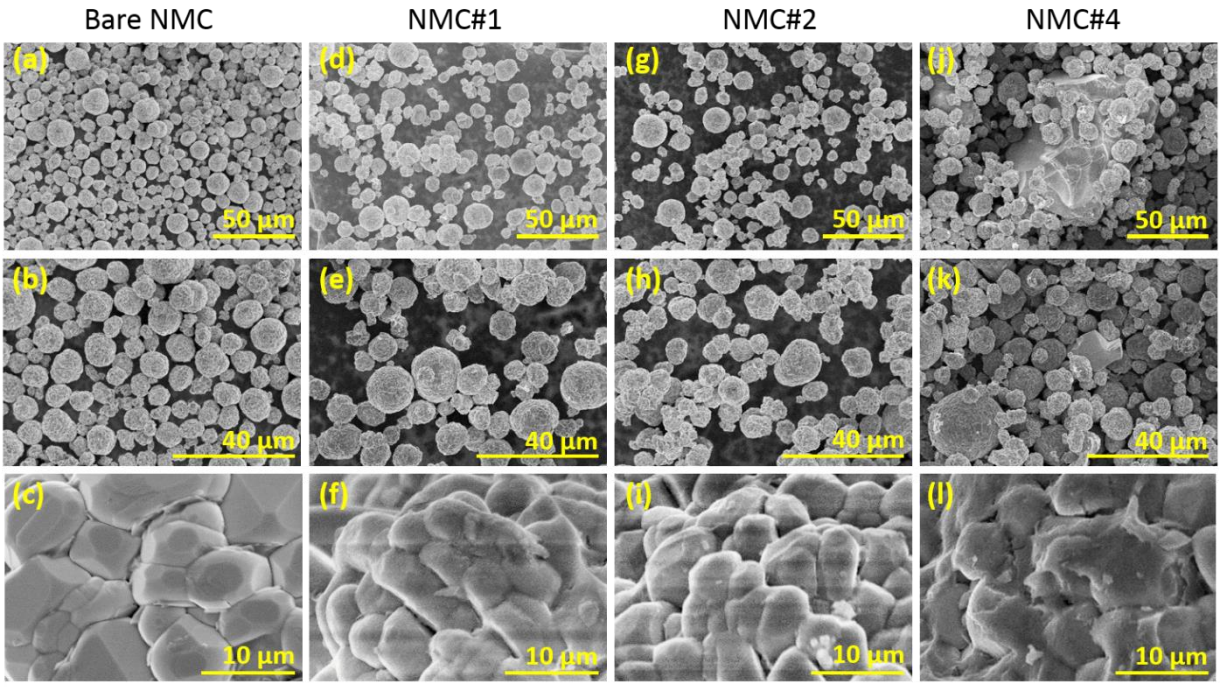

Figure S5. SEM images to show the morphology of NMC with different coating thickness. The morphology of NMC#3 was shown in **Figure 2** in main manuscript.

6. The electrochemical performance of NMC with different coating thickness.

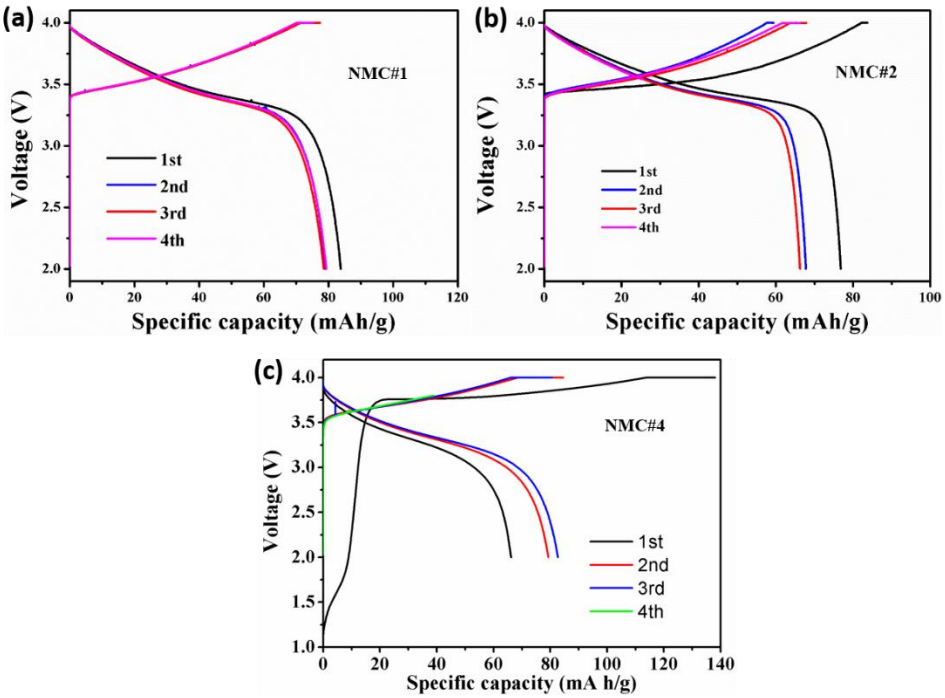

Figure S6. Electrochemical performance of NMC with different coating thickness.

7. The morphology of NMC after ball mill and the corresponding electrochemical performance.

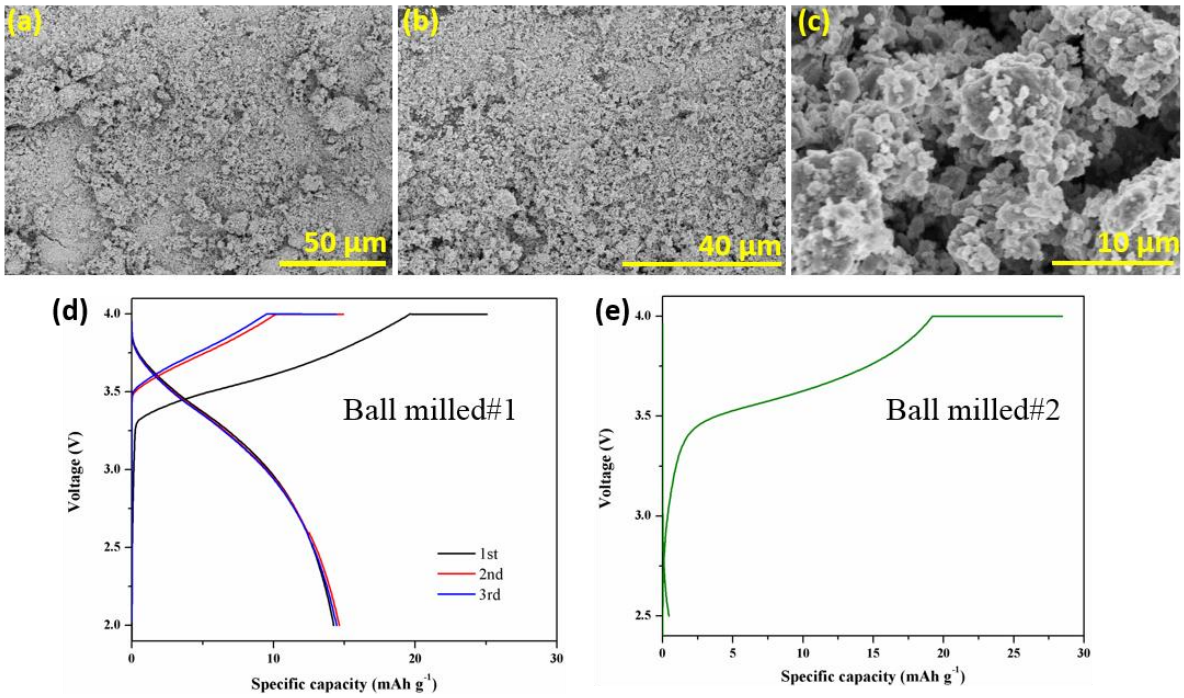

Figure S7. (a-c) Morphology of NMC after ball milling. Electrochemcial performance of NMC: (d) coating first and then ball mill; (e) ball mill first and then applied coating.

8. Charge/discharge profiles in rate measurement.

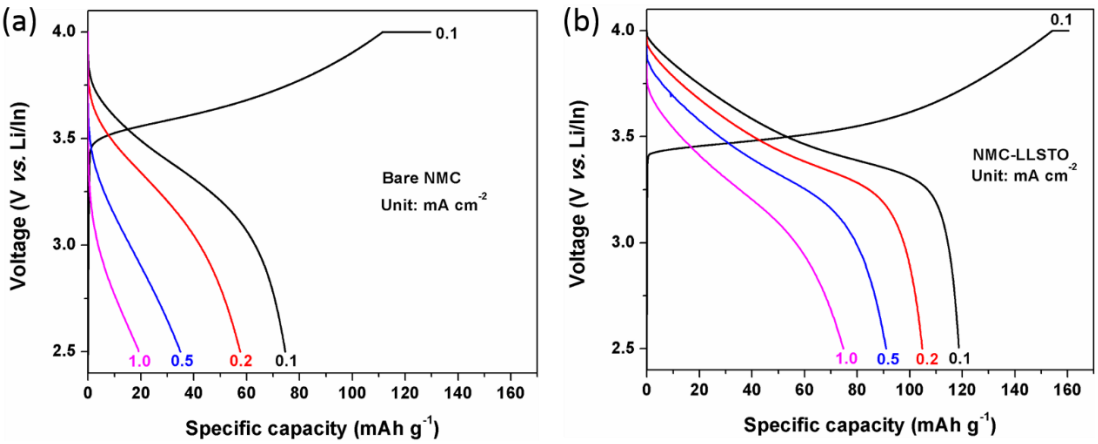

Figure S8. The charge/discharge profiles of (a) Bare NMC and (b) NMC-LLSTO at different rate.

9. Performance comparison

Table S2. The comparison in electrochemical performance of reported ASSLB using $LiNi_{1/3}Mn_{1/3}Co_{1/3}O_2$ (NMC111) cathode and sulfide electrolyte.

No.	Cathode	Coating	Electrolyte	Anode	Cycling performance	Ref.
1	NMC111	LLSTO	Li_6PS_5Cl	In-Li	**53 mA/g, 100 mAh/g, after 650 cycles**	**This work**
2	NMC111	Al_2O_3	Li_3PS_4	$Li_{4.4}Si$	11 mA/g, 113 mAh/g, after 100 cycles	[2]
		$LiAlO_2$	Li_3PS_4	$Li_{4.4}Si$	11 mA/g, 124 mAh/g, after 400 cycles	[2]
3	NMC111	ZrO_2	Li_3PS_4	$Li_{4.4}Si$	7.87 mA/g, 115 mAh/g, after 50 cycles	[3]
4	NMC111	$LiNbO_3$	$75Li_2S \cdot 25P_2S_5$	In-Li	67 mA/g, 126 mAh/g, after 10 cycles	[4]
5	NMC111	$LiNbO_3$	Li_6PS_5Br	In-Li	15.4 mA/g, 87 mAh/g, after 10 cycles	[5]
6	NMC111	$Li_4Ti_5O_{12}$	$80Li_2S \cdot 19P_2S_5 \cdot P_2O_5$	In-Li	16.6 mA/g, 120 mAh/g,	[6]

					after 10 cycles	
7	NMC111	$LiNbO_3$	$75Li_2S$ $25P_2S_5$	In-Li	No cycling	[7]

10. Calculated thermodynamic decomposition energies and phase equilibria

Table S3: Data for NMC | Li_6PS_5Cl pseudobinary, with ratio of Li_6PS_5Cl in pseudobinary, mutual reaction energy between phases at the ratio, and phase equilibria at the ratio.

ratio of Li_6PS_5Cl	mutual reaction energy (eV/atom)	phase equilibria
0.000	0.000	$LiMn_{0.3}Co_{0.3}Ni_{0.3}O_2$
0.004	-0.019	Li_2MnO_3, $LiCoNiO_4$, $Li_7Co_5O_{12}$, Li_3PO_4, $LiClO_4$, Li_2SO_4, NiO
0.016	-0.075	Li_2MnO_3, $Li_7Co_5O_{12}$, Li_3PO_4, $LiClO_4$, Li_2SO_4, $LiCoO_2$, NiO
0.020	-0.091	Li_2MnO_3, LiCl, $Li_7Co_5O_{12}$, Li_3PO_4, Li_2SO_4, $LiCoO_2$, NiO
0.024	-0.105	Li_2MnO_3, LiCl, Li_3PO_4, Li_2SO_4, $LiCoO_2$, NiO, Li_5CoO_4
0.040	-0.140	Li_2MnO_3, LiCl, Li_3PO_4, Ni, Li_2SO_4, $LiCoO_2$, NiO
0.074	-0.208	Li_2MnO_3, LiCl, Li_3PO_4, Mn_3O_4, Ni, Li_2SO_4, $LiCoO_2$
0.077	-0.213	Li_2MnO_3, LiCl, $LiMnO_2$, Ni, Li_3PO_4, Li_2SO_4, $LiCoO_2$
0.111	-0.244	Li_2MnO_3, LiCl, Li_3PO_4, Ni, Co_3Ni, Li_2SO_4, $LiCoO_2$
0.130	-0.261	Li_2MnO_3, LiCl, Li_3PO_4, Ni, Co_3Ni, Li_2SO_4, Li_6CoO_4
0.143	-0.273	LiCl, $LiMnO_2$, Ni, Li_3PO_4, Co_3Ni, Li_2SO_4, Li_6CoO_4
0.149	-0.276	LiCl, $LiMnO_2$, Ni, Li_3PO_4, Co_3Ni, Li_2SO_4, Li_2O
0.152	-0.278	LiCl, $LiMnO_2$, Ni, Li_3PO_4, Co_3Ni, Li_2SO_4, Li_6MnO_4
0.240	-0.302	LiCl, Co_9S_8, $LiMnO_2$, Ni, Li_3PO_4, Li_2SO_4, Li_6MnO_4
0.250	-0.305	LiCl, Co_9S_8, Li_3PO_4, Ni, Li_2SO_4, Li_6MnO_4, MnO
0.302	-0.317	Ni_3S_2, LiCl, Co_9S_8, Li_3PO_4, Li_2SO_4, Li_6MnO_4, MnO
0.446	-0.344	Ni_3S_2, LiCl, Co_9S_8, Li_3PO_4, Li_2S, Li_2SO_4, MnO
0.500	-0.343	Ni_3S_2, LiCl, Li_3PO_4, MnO, Li_2S, Li_2SO_4, Co_2NiS_4
0.520	-0.342	$Co(NiS_2)_2$, LiCl, Li_3PO_4, MnO, Li_2S, Li_2SO_4, Co_2NiS_4
0.613	-0.333	$Co(NiS_2)_2$, MnS_2, LiCl, Li_3PO_4, Li_2S, Li_2SO_4, Co_2NiS_4
0.624	-0.327	MnS_2, LiCl, S_8O, Li_3PO_4, Li_2S, $Co(NiS_2)_2$, Co_2NiS_4
0.625	-0.326	MnS_2, LiCl, CoS_2, Li_3PO_4, Li_2S, $Co(NiS_2)_2$
1.000	0.000	Li_6PS_5Cl

Table S4: Data for NMC | LLSTO pseudobinary, with ratio of LLSTO in pseudobinary, mutual reaction energy between phases at the ratio, and phase equilibria at the ratio.

ratio of LLSTO	mutual reaction energy (eV/atom)	phase equilibria
0.000	0.0000	$LiMn_{0.3}Co_{0.3}Ni_{0.3}O_2$
0.029	-0.0009	$SrTiO_3$, La_2TiO_5, $LiCoNiO_4$, Li_2TiO_3, NiO, $Li_7Co_5O_{12}$, Li_2MnO_3
0.107	-0.0032	$SrTiO_3$, La_2TiO_5, $LiCoO_2$, $LiCoNiO_4$, Li_2TiO_3, NiO, Li_2MnO_3
0.191	-0.0046	$SrTiO_3$, $Li(CoO_2)_2$, La_2TiO_5, $LiCoNiO_4$, Li_2TiO_3, NiO, Li_2MnO_3
0.307	-0.0059	$SrTiO_3$, $Li(CoO_2)_2$, $LiCoNiO_4$, Li_2TiO_3, NiO, Li_2MnO_3, $La_2Ti_2O_7$
0.571	-0.0080	$SrTiO_3$, $Li(CoO_2)_2$, $LiCoNiO_4$, Li_2TiO_3, NiO, $Li_2Mn_3NiO_8$, $La_2Ti_2O_7$
0.586	-0.0078	$SrTiO_3$, $Li(CoO_2)_2$, $Ti_4(Ni_5O_8)_3$, $LiCoNiO_4$, Li_2TiO_3, $Li_2Mn_3NiO_8$, $La_2Ti_2O_7$
0.790	-0.0052	$SrTiO_3$, $SrLi_2Ti_6O_{14}$, $Li(CoO_2)_2$, $LiCoNiO_4$, Li_2TiO_3, $Li_2Mn_3NiO_8$, $La_2Ti_2O_7$
0.822	-0.0046	$SrLi_2Ti_6O_{14}$, $Li(CoO_2)_2$, O_2, $LiCoNiO_4$, Li_2TiO_3, $Li_2Mn_3NiO_8$, $La_2Ti_2O_7$
1	0.0000	$Li_{0.35}La_{0.5}Sr_{0.05}TiO_3$

Table S5: Data for Li_6PS_5Cl | LLSTO pseudobinary, with ratio of LLSTO in pseudobinary, mutual reaction energy between phases at the ratio, and phase equilibria at the ratio.

ratio of LLSTO	mutual reaction energy (eV/atom)	phase equilibria
0.000	0.0000	Li_6PS_5Cl
0.334	-0.0811	LaS_2, Li_4TiS_4, Li_2S, SrS, Li_3PO_4, LiCl, $Li(TiS_2)_2$
0.358	-0.0799	LaS_2, Li_2S, SrS, Li_3PO_4, LiCl, Li_2TiO_3, $Li(TiS_2)_2$
0.418	-0.0766	LaS_2, Li_2S, Li_3PO_4, Li_2TiO_3, LiCl, $Sr(LaS_2)_2$, $Li(TiS_2)_2$
0.477	-0.0733	LaS_2, Li_3PO_4, Li_2TiO_3, LiCl, $La_{10}S_{19}$, $Sr(LaS_2)_2$, $Li(TiS_2)_2$
0.478	-0.0733	LaS_2, $La_{10}S_{14}O$, Li_3PO_4, Li_2TiO_3, LiCl, $Sr(LaS_2)_2$, $Li(TiS_2)_2$
0.549	-0.0678	$SrLi_2Ti_6O_{14}$, LaS_2, $La_{10}S_{14}O$, Li_3PO_4, LiCl, Li_2TiO_3, $Li(TiS_2)_2$
0.721	-0.0544	$SrLi_2Ti_6O_{14}$, LaS_2, $La_{10}S_{14}O$, Li_3PO_4, $Li_4Ti_5O_{12}$, LiCl, Li_2TiO_3
0.774	-0.0488	$SrLi_2Ti_6O_{14}$, LaS_2, Li_3PO_4, $Li_4Ti_5O_{12}$, Li_2TiO_3, LiCl, $La_4Ti_3(SO_2)_4$
0.950	-0.0241	$SrLi_2Ti_6O_{14}$, LaS_2, Li_3PO_4, $Li_4Ti_5O_{12}$, Li_2TiO_3, LiCl, $La_2Ti_2O_7$
0.997	-0.0159	$SrLi_2Ti_6O_{14}$, Li_3PO_4, $Li_4Ti_5O_{12}$, Li_2TiO_3, LiCl, Li_2SO_4, $La_2Ti_2O_7$
0.997	-0.0138	$SrLi_2Ti_6O_{14}$, Li_3PO_4, $LiClO_4$, $Li_4Ti_5O_{12}$, Li_2TiO_3, Li_2SO_4, $La_2Ti_2O_7$

1.000	0.0000	$Li_{0.35}La_{0.5}Sr_{0.05}TiO_3$

Reference

1. Cui, S.; Wei, Y.; Liu, T.; Deng, W.; Hu, Z.; Su, Y.; Li, H.; Li, M.; Guo, H.; Duan, Y.; Wang, W.; Rao, M.; Zheng, J.; Wang, X.; Pan, F. *Advanced Energy Materials* **2016,** 6, (4), 1501309.
2. Okada, K.; Machida, N.; Naito, M.; Shigematsu, T.; Ito, S.; Fujiki, S.; Nakano, M.; Aihara, Y. *Solid State Ionics* **2014,** 255, 120-127.
3. Machida, N.; Kashiwagi, J.; Naito, M.; Shigematsu, T. *Solid State Ionics* **2012,** 225, 354-358.
4. Sakuda, A.; Takeuchi, T.; Kobayashi, H. *Solid State Ionics* **2016,** 285, 112-117.
5. Chida, S.; Miura, A.; Rosero-Navarro, N. C.; Higuchi, M.; Phuc, N. H. H.; Muto, H.; Matsuda, A.; Tadanaga, K. *Ceramics International* **2018,** 44, (1), 742-746.
6. Kitaura, H.; Hayashi, A.; Tadanaga, K.; Tatsumisago, M. *Electrochim Acta* **2010,** 55, (28), 8821-8828.
7. Asano, T.; Yubuchi, S.; Sakuda, A.; Hayashi, A.; Tatsumisago, M. *J Electrochem Soc* **2017,** 164, (14), A3960-A3963.